Application of Ion-Impact Energy Measurement to Electrospray Ionization Mass Spectrometry of Proteins and Protein Mixtures

M. W. Rabin, G. C. Hilton, and John M. Martinis
National Institute of Standards and Technology, Boulder, Colorado, USA

We have used a normal metal-insulator-superconductor (NIS) microcalorimeter to measure the impact energy of protein ions produced by electrospray ionization (ESI) in a magnetic-sector mass spectrometer (MS). We have used these measurements to resolve spectral ambiguities and to analyze protein mixtures. Energy measurement may be useful for the direct MS analysis of complex biopolymer mixtures that normally would confound ESI-MS deconvolution algorithms. (J Am Soc Mass Spectrom 2001, 12, 826–831) Published by Elsevier Science Inc.

The possibility of improving the sensitivity of biopolymer mass spectrometry (MS) at high mass ($m > 100$ kDa) has inspired several recent experiments using low-temperature detectors (LTDs) based on superconducting devices [1]. LTDs have three potential advantages over conventional ion detectors: (1) high quantum efficiency for ion detection independent of ion mass (m); (2) extremely low noise due to low detector and preamplifier operating temperatures ($T < 1$ K and $T \sim 4$ K, respectively); and (3) the measurement of ion-impact energy (E_I), which is proportional to ion-kinetic energy ($E_I \propto E_K$). At present, there are drawbacks to the use of LTDs, such as the small detector area ($\lesssim 0.1$ mm^2), difficulties of low-temperature operation, and long recovery times (~ 1 to 15 μs, depending on design). Previous experiments have measured E_I of proteins [2, 3], compared LTD and microchannel plate (MCP) performance [4, 5, 6], analyzed oligonucleotides [7], and identified microorganisms [8].

Our work emphasizes the measurement of E_I to complement the spectrometer's determination of mass-to-charge ratio, m/z (where z is the number of elementary charges). The measurement of E_I might be especially useful in electrospray ionization (ESI) MS because ESI produces ions with many charge states, hence many values of E_K. The measurement of E_I provides an additional axis in the spectrum; instead of just an m/z spectrum (intensity vs. one variable), we have a combined m/z and E_I spectrum (intensity vs. two variables). The quality of the combined spectrum depends on two parameters: the mass-to-charge ratio resolution ($R_{m/z} = (m/z)/\Delta(m/z)$) and energy resolution ($R_E = E_I/\Delta E_I$), where $\Delta(m/z)$ and ΔE_I are the respective full-widths at half-maximum (FWHMs).

In this article, we present experimental results from the ESI-MS of proteins using a normal metal-insulator-superconductor (NIS) microcalorimeter as the ion detector. Using the m/z and E_I spectrum, we resolve spectral ambiguities that cannot be resolved using a conventional MS detector and investigate the nonlinearity of the ion-absorber interaction. We also report the first results of the ESI-MS analysis of a protein mixture using an energy resolving detector.

Experimental

We have performed ESI-MS analyses of proteins and protein mixtures. All chemicals (bought from SIGMA, St. Louis, MO) [9] were dissolved in a solution of deionized-water:methanol:acetic acid (50:50:3) without further purification. The ESI source (Analytica of Branford) [9] follows the classic design of Fenn [10], and injects ions into a magnetic-sector mass spectrometer (JEOL HX110) [9]. The flow rate into the ESI atmospheric chamber was ~8 to 30 nl/s (0.5 to 2 μl/min), where there was a countercurrent flow of N_2 gas at ~0.06 1/s and ~420 K. The ESI needle was either a fused silica capillary (50 μm i.d.) or a stainless steel capillary (100 μm i.d.) operated at 2 kV to 3 kV above the (grounded) MS inlet with a spray current of 50 to 100 nA. The accelerating voltage was 4 kV, and electrostatic quadrupole lenses maximized ion transmission. By adjusting the collector slit, we can control the $R_{m/z}$, typically operating with $R_{m/z} = 1000$ to 3000. m/z spectra were obtained by sweeping the magnetic field over a range corresponding to $m/z = 1$ kDa to 5 kDa. The spectrometer is equipped with two detectors. The first is a conventional charge-cascade detector: a conversion dynode and electron multiplier. The second is our NIS microcalorimeter. We can electrostatically switch between

Published online May 4, 2001
Address reprint requests to M. W. Rabin, Optoelectronics Division, National Institute of Standards and Technology, 325 Broadway (MC 815.03), Boulder, CO 80305-3328. E-mail: rabin@boulder.nist.gov

1044-0305/01/$20.00
PII S1044-0305(01)00254-9

Received December 8, 2000
Revised February 26, 2001
Accepted March 2, 2001

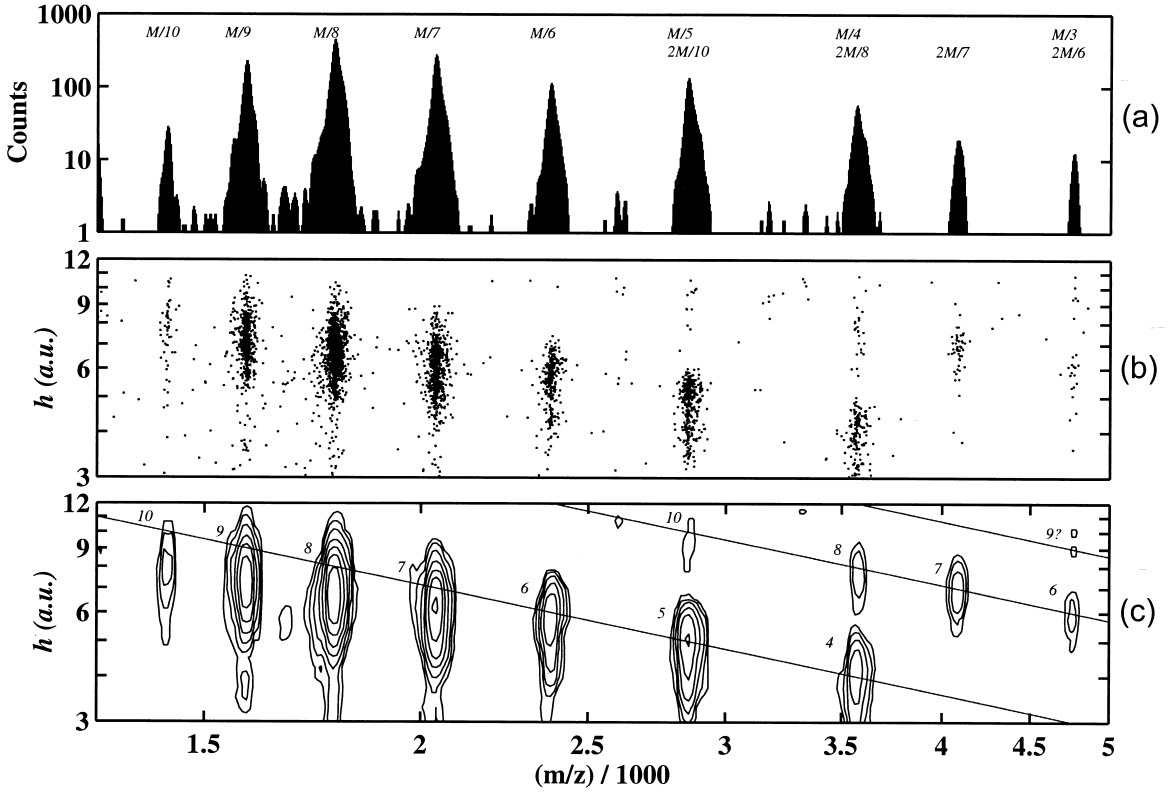

Figure 1. ESI-MS analysis of lysozyme: (**a**) *m/z* spectrum, (**b**) *m/z*-h scatter plot, and (**c**) *m/z*-h contour plot, all using logarithmic horizontal and vertical axes. The density of ion strikes in the *m/z*-h plane doubles with each contour interval. The lines of constant mass at km_{Lys} are $\log(h) = \log(km_{Lys}) - \log(m/z)$ with k = 1, 2, 3, from bottom to top. Each peak in (**c**) is labeled by its charge.

the two detectors. An electrostatic double quadrupole and deflector plates concentrated the ion beam onto the NIS detector. All the data presented in this article were taken using the NIS detector. Typical count rates on a peak were ~100/s, and the typical analysis time was ~1000 s. (Using the large-area conversion dynode detector, analysis times of about 60 s are required to obtain comparable statistics.)

Our NIS microcalorimeter is based on designs that have been described previously [3]. Microcalorimeters absorb and thermalize incident energy ($E_K \sim$ fJ), causing a temperature increase ($\Delta T \sim$ mK) of the absorbing element, which has a small heat capacity ($C \sim$ pJ/K) and sits on a silicon nitride membrane (which provides thermal isolation). The heat then escapes through a thermal conductance ($G \sim 100$ nW/K) to a cold thermal bath ($T_b \sim 100$ mk). A sensitive thermometer measures ΔT, which is proportional to the absorbed energy. When an ion strikes the NIS's normal-metal absorber (350 μm × 350 μm × 200 nm Ag film), a fraction of the ion's E_K is thermalized, depositing energy E_I into the electrons of the Ag film. The subsequent ΔT produces a current pulse $\Delta I(t)$ in the voltage-biased NIS junction. In this case, the absorber is an integral part of the thermometer, and $\Delta I(t)$ is measured using a low-noise 1 MHz bandwidth series-array superconducting-quantum-interference-device amplifier [11]. The detector's effective 1/e fall-time constant is ~12 μs, and the energy resolution for 6 keV x-rays is ~100 eV. From previous experiments [3], we know the X-ray energy is completely thermalized, providing a calibration; for protein molecular ions, however, only about half of the kinetic energy is thermalized, i.e., $E_I \sim E_K/2$. So the peak height of the pulses is half of what we expect given complete thermalization of the kinetic energy, as seen previously in Ref. [3]. After digitally sampling each pulse, we extracted the pulse height (h) using optimal filtering and correcting for a small dc offset (~1% of total signal). For linear energy response, $h \propto E_I \propto E_K$, and we have scaled h so that h = 1 corresponds to the energy of a z = 1 ion.

Results

Using only the *m/z*-spectrum, it is sometimes impossible to unambiguously attribute some *m/z*-peaks to one species if the sample contains monomers ($m = m_1$), dimers ($m = 2m_1$), trimers ($m = 3m_1$), etc., because $m_1/z = 2m_1/2z = 3m_1/3z = \ldots$. Figures 1 and 2 illustrate how this ambiguity is resolved using E_I measurement for the protein lysozyme, with mass m_{LYS} = 14305 Da. In the conventional *m/z* spectrum (Figure 1a), there are peaks at m_{LYS}/z for z = +3 to +10 and one at $2m_{Lys}/7$. Figure 1b shows a scatter plot of h vs. *m/z*; each small dot corresponds to a single ion strike, with a

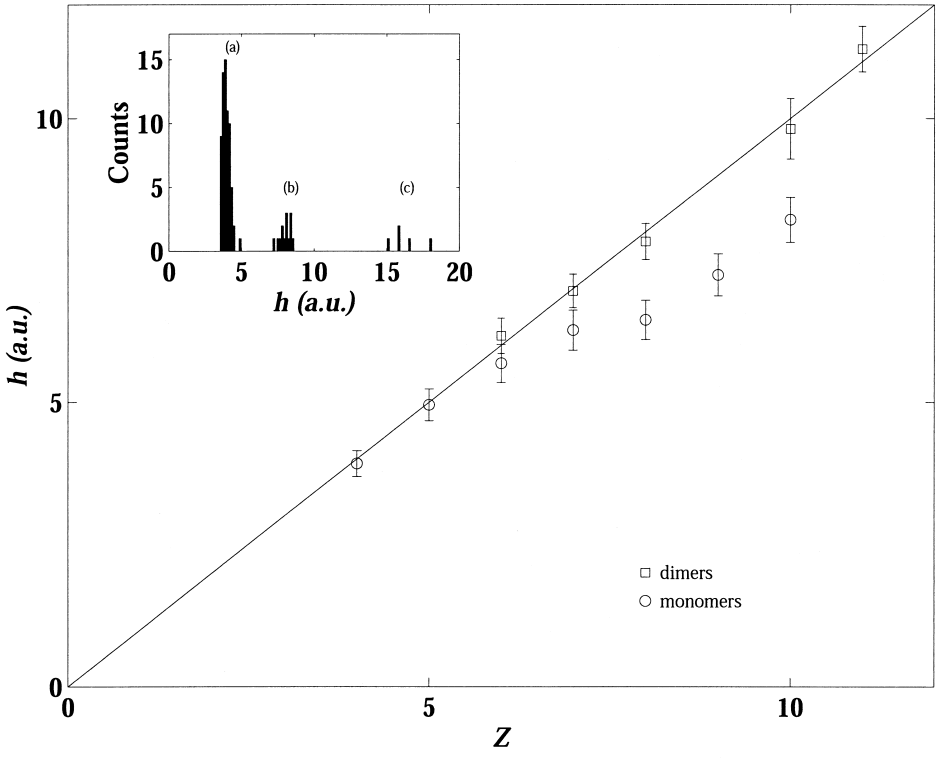

Figure 2. Plot of h vs. z for lysozyme monomers (circles) and dimers (squares) showing sublinear response for the monomers. The line is a least-squares best fit to the dimer data. Inset: h spectrum for lysozyme at fixed m/z = 3575 Da showing (**a**) major peak due to lysozyme monomer with z = +4, (**b**) minor peak due to lysozyme dimer with z = +8, and (**c**) a higher energy group of ions possibly due to lysozyme tetramers with z = +16.

measurement of both h and m/z. The same data are shown in a contour plot in Figure 1c; the contours indicate the density of ion strikes in m/z-h plane, with density doubling with each contour interval. We attribute seven peaks in the m/z-h plane to the lysozyme monomer (z = +4 to +10), and three to the dimer (z = +6 to +8). There are also faint groupings that might be the +10 dimer and the +9 trimer. Assuming $h \propto z$, $\ln(h) = \ln(k) + \ln(m) - \ln(m/z)$, where k is a constant, so we expect the peaks in the m/z-h plane corresponding to a common mass (fixed m) to fall on a line of slope −1 on a log-log plot. The $m = m_{LYS}$ line of constant mass does not pass through the centers of the lysozyme monomer peaks, instead it passes above them at higher energy, suggesting a departure from linear response (see below). The $m = 2m_{Lys}$ line passes through the z = +6, +7, +8, and +10 dimer peaks. There is no cluster of points on the $m = m_{Lys}$ line at z = +3, suggesting that the peak at $m/z = m_{Lys}/3$ is dominated by $m = 2m_{Lys}$, z = +6 ions. Alternatively, the $m = 2m_{Lys}$, z = +6 ion strikes could be caused by the simultaneous arrival of two monomers with z = +3, but this is inconsistent with the low count rates (<1000/s) in these experiments and the absence of high-energy ion strikes for the dominant peaks, e.g., no $h \sim 16$ (z = +16) events above the $h \sim 8$ (z = +8) peak at $m/z = m_{Lys}/8$. The $2m_{Lys}$ and m_{Lys} lines of constant mass clearly separate, and the two components can be identified even in the presence of noise with very few counts.

The inset to Figure 2 shows the h spectrum for a second lysozyme solution for a narrow range around m/z = 3575 Da, with $\Delta(m/z) \sim 10$ Da. This m/z-range corresponds to the +4 monomer, +8 dimer, etc. Ion strikes on the silicon nitride membrane (which supports the microcalorimeter) have been removed from these data using the pulse-shape and pulse-height correlation outlined in Ref. [2]. The E spectrum divides into three well separated regions: (a) $3.5 < h < 4.9$, (b) $7.2 < h < 8.5$, and (c) $h > 15$. The major peak, region (a), has a mean pulse height of $h_a = 3.95$. The minor peak, region (b), has a mean pulse height of $h_b = 8.04$. The few ion strikes at high-energy, region (c), do not form a well-defined peak, but have a mean pulse height of $h_c = 16.3$. The mean pulse heights are nearly in integer ratios: $h_b/h_a = 2.0$ and $h_c/h_a = 4.1$. Since h_a matches the expected value for the +4 charge state, the integer ratios of the peak heights suggest that the minor peak (b) is due to lysozyme dimers and that the high-energy region (c) is possibly due to lysozyme tetramers. The presence of the lysozyme dimer is confirmed by $m = 2m_{Lys}$ and z = 6, 7 and 10 peaks (e.g. Figure 1b and 1c). No such confirmation is found for the lysozyme tetramer.

It is important to note two features of these results. First, even in the presence of undetermined chemical

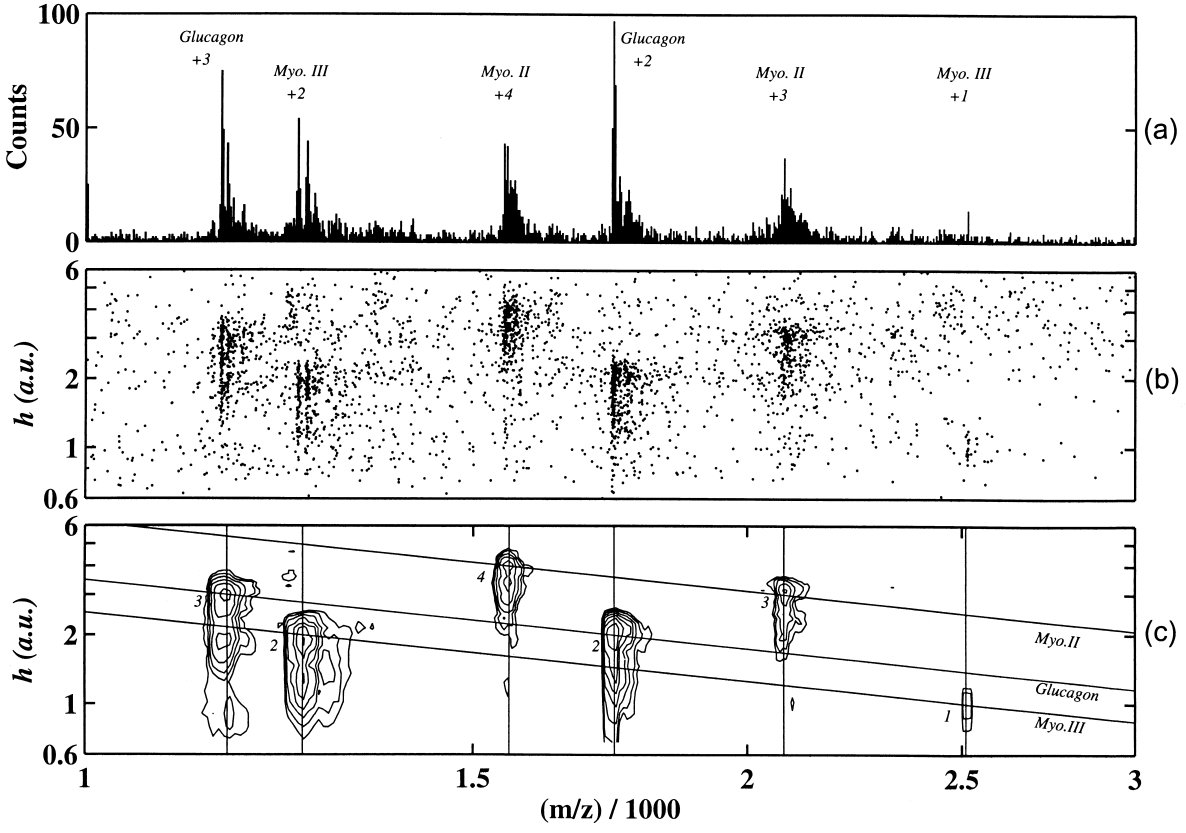

Figure 3. ESI-MS analysis of a mixture of myoglobin digestion products and glucagon: (**a**) *m/z* spectrum (linear vertical axis and logarithmic horizontal axis), (**b**) *m/z*-h scatter plot (logarithmic axes), and (**c**) *m/z*-h contour plot (logarithmic axes). The density of ion strikes in the *m/z*-h plane doubles with every two contour intervals. The lines of constant mass at M_X are $\log(h) = \log(m_X) - \log(m/z)$ with $m_X = m_{III}$, m_G, and m_{II}, from bottom to top. Each peak in (**c**) is labeled by its charge.

noise, the ultra-low-noise performance of the detector allows us to resolve the monomer-dimer ambiguity in the *m/z* spectrum ($m_1/z = 2m_1/2z$) even with very few total counts. The spaces between regions (a)–(c) in Figure 2a are empty, indicating an absence of noise counts. Second, this type of ambiguity cannot be resolved using a conventional ion detector, although, of course, the presence of the dimer can be inferred from the peaks in the *m/z* spectrum with odd-integer charge.

By combining data from two lysozyme experiments we get a clearer picture of the departure from linear response mentioned previously. In Figure 2 we plot h vs. z, where z is inferred from the *m/z* spectrum. Assuming $z \propto E_K$ and $E_I \propto h$, we can compare the energy deposited in the detector by the monomers and dimers at fixed E_K. Consistent with Figure 1, the energy deposited by the dimers is nearly linear up to $z \sim 10$, i.e., $E_K \sim 40$ keV. For $z = 4$ and 5, the monomer data fall on the same line, but above $z = 7$, the response is sublinear. Analyses of lighter molecules that produce lower charge ions show h(z) to be linear for $z = 1$ to 4. Because h(z) is linear for the dimers, the microcalorimeter's conversion of a heat impulse into a current pulse is not significantly nonlinear at these energies. Instead, the source of the nonlinearity must be in the interaction of the ion with the absorber, i.e., $E_I(E_K)$ is sublinear for the monomers, and E_I depends on more than just E_K. Future work could study E_I as a function of species, m, E_K, and z. It would be very interesting to use charge-reduction methods [12, 13] to study the ion-absorber interaction at lower z for high-m molecules (e.g., $z < 4$ for lysozyme).

The measurement of E_I could be useful in the direct ESI-MS analysis of biopolymer mixtures by increasing the separation between peaks. In an initial attempt to do this, we have conducted the first ESI-MS analyses of biopolymer mixtures using a cryogenic detector. The mixture consisted of myoglobin fragments (including myoglobin I, II, and III, masses $m_I = 8160$ Da, $m_{II} = 6210$ Da and $m_{III} = 2510$ Da, respectively) and glucagon ($m_G = 3480$ Da). This mixture is normally used for the calibration of protein gel electrophoresis (SIGMA MWM-SDS-17s) [9], and our solution had a nominal concentration of 220 μg/ml. Figure 3 shows the resulting *m/z* spectrum, *m/z*-h scatter plot, and *m/z*-h contour plot. There is considerable chemical noise and few total counts (~3500). Nonetheless, we can identify three components of the mixture. In the *m/z* spectrum there are peaks (in order of increasing *m/z*) at $m_G/3$, $m_{III}/2$, $m_{II}/4$, $m_G/2$, $m_{II}/3$, $m_{III}/1$, and their Na adducts. The Na adducts are not resolved in the contour plot due to

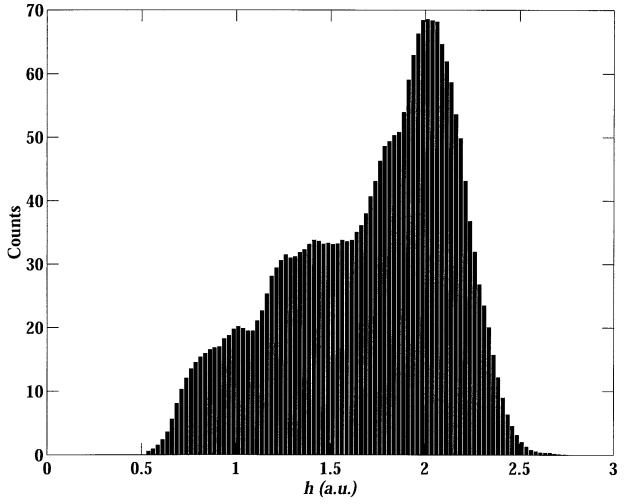

Figure 4. h spectrum of glucagon at fixed m/z = 1745 Da, i.e., z = 2. Three broad, low-energy shoulders are clear. We used a five-point smoothing filter over 100 bins, so the effective binwidth is $\Delta h = 0.125$.

the two-dimensional binning required to construct the contours in the presence of substantial chemical noise and few total counts. The presence of the weak peak at $m = m_{III}$ and $z = 1$ was confirmed by taking an h spectrum at fixed m/z. In the contour plot, the lines of constant mass for m_G, m_{II}, and m_{III} intersect the corresponding m/z-h peaks. Though these peaks can be distinguished in the m/z spectrum, the contour plot shows how lines of constant mass can be used to increase the separation between the peaks of a complex biopolymer mixture. This additional separation could be especially useful in the direct analysis of mixtures containing more than about seven components because standard ESI-MS deconvolution algorithms break down as spectral complexity and chemical noise increase [12, 13]. Mixtures of this kind are today analyzed using LC-MS and LC-MS-MS. Future work could apply E measurement to such complex mixtures, potentially containing minor components that would be missed in conventional ESI MS using only an m/z spectrum.

Our ability to separate the components of a mixture depends on both $R_{m/z}$ and R_E. As clearly shown from Figures 1 to 3, peaks that are close in m/z but significantly different in z can easily be resolved, e.g., monomers and dimers of identical m/z with $\Delta z \geq 3$ at $z \lesssim 10$. But the peaks in the m/z-h plane are quite broad in h, in all cases having $R_E < 5$, limiting the utility of our methods. To estimate R_E we use h spectra at a fixed m/z corresponding to a known peak, such as that of the $z = +2$ glucagon ion at $m/z = 1745$ shown in Figure 4. Three broad, low-energy shoulders are clear. The origin of these shoulders is unclear, but we believe them to be features of the ion-absorber interaction. Similar but less pronounced features are seen at other charges and masses and with glucagon and other proteins. On the low-energy side of the peak, the fall to half-height occurs over $\Delta h \sim 0.38$. The drop off on the high-energy side is more rapid and smooth, with the fall to half-height occurring over $\Delta h \sim 0.25$. Combining these values, we find $\Delta h_{FWHM} \sim 0.7$ and $R_E \sim 3$. The presence of the broad shoulders makes R_E a less useful quantity for parameterizing the response of our detector than it is for h spectra that are free of such artifacts.

Assuming that future detector designs can reduce R_E and produce E_I spectra without significant artifacts, we need to establish some criteria for energy measurement to be useful. To do this, we consider the specific problem of ESI-MS analysis of a DNA-ladder sample containing all fragment lengths from N = 1 to 400 nucleotides (nt). Each fragment will produce many peaks in the m/z-E plane; our ability to separate these peaks depends on both $R_{m/z}$ and R_E. Considering only separation in E_I, we naively estimate that $R_E \gtrsim 2z \sim 80$ is required to resolve the peaks. But our simulations, e.g., the one shown in Figure 5 , show that R_E substantially lower than 80 is sufficient to identify all the components of the mixture. This example simulation generates over 3800 peaks in the m/z-E_I plane in the range m/z = 1 kDa to 5 kDa and z = 1 to 30, assuming $R_{m/z} = 1200$ and $R_E = 40$, and $h = E_I = E_K = z$. Using these parameters, the simulation randomly generates 400 points (i.e., 400 ion strikes) in the m/z-E_I plane for each peak. The narrow m/z window shown in Figure 5 contains 96 peaks that remain unresolved in the conventional m/z spectrum. From the scatter and contour plots, many peaks can be resolved by eye. Peaks that are close in m/z and E_I in the scatter plot, e.g., in the upper right corner of Figure 5b, cannot easily be resolved by eye, but are resolved in the contour plot. More detailed calculations show that $R_E \gtrsim 30$ and $R_{m/z} \gtrsim 1000$ will resolve all of the >3800 peaks [14]. Furthermore, to compete in mass range with current matrix-assisted laser desorption/ionization time-of-flight DNA sequencing experiments, we need $R_E \sim 10$ to 20 [14–16]; to compete in mass range with electrophoresis at $N \sim 300$, we need $R_E \gtrsim 30$. These simulation results establish a criterion ($R_E \gtrsim 30$) for R_E for a specific problem and imply that less challenging problems, e.g., smaller N or a less tightly congested spectrum from a protein mixture, would be tractable with less stringent criteria for R_E.

Conclusions

We have successfully analyzed proteins and protein mixtures using ESI-MS with a microcalorimeter ion detector. The measurement of E_I has resolved spectral ambiguities between lysozyme monomers and dimers. The nonlinearity in the h vs. z curve for lysozyme monomers is due to the ion-absorber interaction, and is not due to nonlinearity of the microcalorimeter. Analysis of a protein mixture demonstrates how E measurement provides additional separation between components of the mixture. Future work should concentrate on improving R_E, studying E_I as a function of species, m, E_K, and z (possibly using charge reduction), and applying E measurement to biopolymer mixtures. Since the energy resolution for biopolymer ions is so far

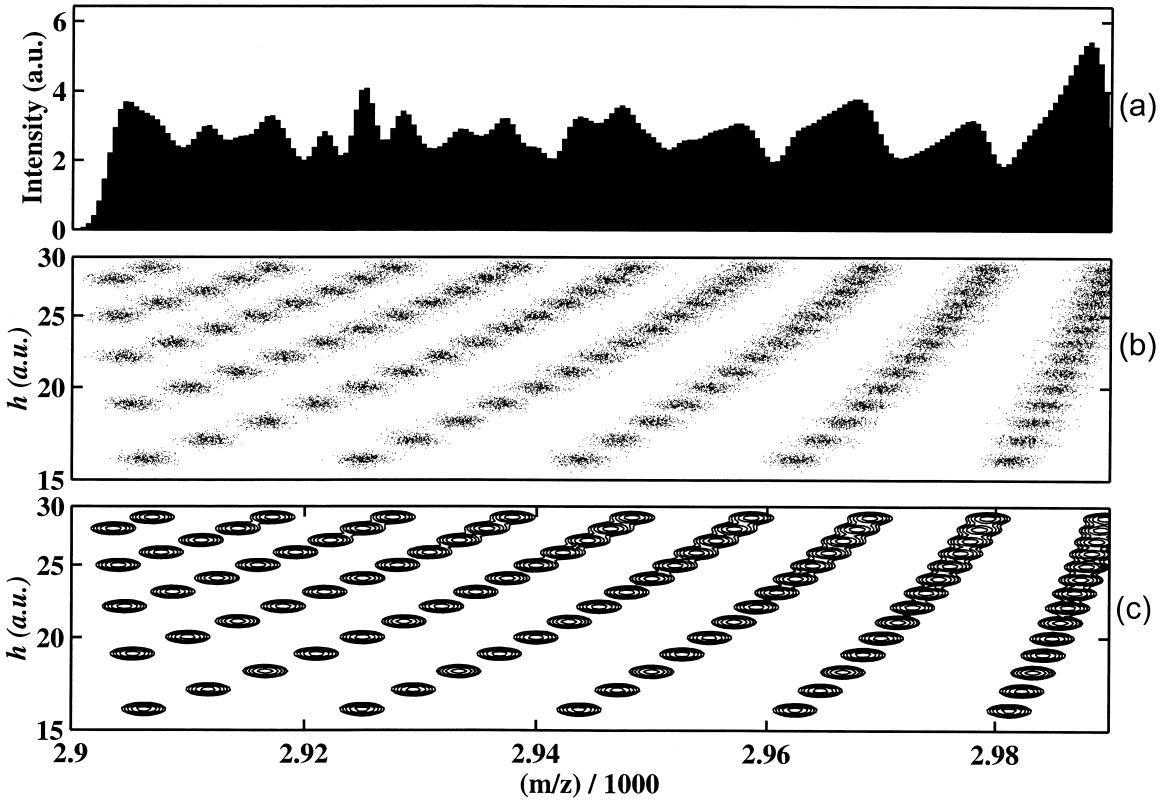

Figure 5. Results of simulation of the ESI-MS analysis of a DNA ladder sample using E measurement: (**a**) *m/z* spectrum (linear vertical axis and logarithmic horizontal axis), (**b**) *m/z*-h scatter plot (logarithmic axes), and (**c**) *m/z*-h contour plot (logarithmic axes). The density of ion strikes in the *m/z*-h plane doubles with every two contour intervals. The simulation assumes $R_E = 40$, $R_{m/z} = 1200$, and $h = E_I = E_K$. All values of N from 1 to 400 nt are included in this simulation, producing ~14 peaks for each value of N. Only a limited portion of the *m/z*-h plane is shown, containing 96 peaks in a 90 Da interval around *m/z* = 2945 Da; for these peaks, N ~ 155 to 289, i.e., m ~ 46 kDa to 87 kDa.

limited by the ion-absorber interaction, we do not expect significant differences in energy resolution between MALDI and ESI ions. Furthermore, the energy resolution of superconducting tunnel junctions as ion detectors is similar [4] to that of our NIS microcalorimeter because both are limited by the ion-absorber interaction. If R_E can be increased by redesigning the absorbing element of the detector, to $R_E \sim 30$, then the measurement of E_I would become very useful for the direct ESI-MS analysis of biopolymer mixtures, specifically for the analysis of DNA ladder samples.

Acknowledgments

The authors thank Prof. Klaus Biemann and Massachusetts Institute of Technology for the donation of the mass spectrometer used in this work. This work was supported by the NIST Advanced Technology Program, and MWR was supported by NIST-National Research Council and NIST-University of Colorado post-doctoral research associateships.

References

1. Frank, M.; Labov, S. E.; Westmacott, G.; Benner, W. H. *Mass Spectrometry Reviews* **1999,** *18*, 155–186.
2. Rabin, M. W.; Hilton, G. C.; Martinis, J. M. *IEEE Transactions on Applied Superconductivity*, in press.
3. Hilton, G. C., et al. *Nature* **1998,** *391*, 672–675.
4. Westmacott, G., et al. *Rapid Commun. Mass Spectrom.* **2000,** *14*, 600–607.
5. Westmacott, G.; Frank, M.; Labov, S. E.; Brenner, W. H. *Rapid Commun. Mass Spectrom.*, **2000,** *14*, 1854–1861.
6. Gervasio, G., et al. *Nuclear Instruments and Methods in Physics Research A* **2000,** *444*, 389–394.
7. Twerenbold, D., et al. *Applied Physics Letters* **1996,** *68*, 3503.
8. Ullom, J. N., et al. *Nuclear Instruments and Methods in Physics Research A* **2000,** *444*, 385–388.
9. These identifications are provided for complete technical description and do not imply recommendation or endorsement by NIST or the United States Government.
10. Fenn, J. B.; Mann, M.; Meng, C. K.; Wong, S. F.; Whitehouse, C. M. *Science* **1989,** *246*, 64–71.
11. Welty, R. P.; Martinis, J. M. *IEEE Transactions on Magnetics* **1991,** *27*, 2924–2926.
12. Scalf, M.; Westphall, M. S.; Krause, J.; Kaufman, S. L.; Smith, L. M. *Science* **1999,** *283*, 194–197.
13. Scalf, M.; Westphall, M. S.; Smith, L. M. *Analytical Chemistry* **2000,** *72*, 52–60.
14. Rabin, M. W.; Hilton, G. C.; Martinis, J. M. Unpublished.
15. Taranenko, N. I., et al. *Nucleic Acid Research* **1998,** *26*, 2488–2490.
16. Yates, J. R. *J. Mass Spectrom.* **1998,** *33*, 1–19.